Chapter 15

Soft-Error Rate of Advanced SRAM Memories: Modeling and Monte Carlo Simulation

Jean-Luc Autran, Sergey Semikh, Daniela Munteanu,
Sébastien Serre, Gilles Gasiot and Philippe Roche

Additional information is available at the end of the chapter

http://dx.doi.org/10.5772/50111

1. Introduction

Single-event-effects (SEE) are the result of the interaction of highly energetic particles, such as protons, neutrons, alpha particles, or heavy ions, with sensitive regions of a microelectronic device or circuit [1-2]. They may perturb the device/circuit operation (e.g., reverse or flip the data state of a memory cell, latch, flip-flop, etc.) or definitively damage the circuit (e.g. gate oxide rupture, destructive latch-up events).

With the constant downscaling of microelectronic devices, the sensitivity of integrated circuits to natural radiation coming from the space or present in the terrestrial environment has been found to seriously increase [3-5]. In particular, ultra-scaled memory integrated circuits are more sensitive to single-event-upset (SEU) and digital devices are more subjected to digital single-event transient (DSETs). The problem has been well-known for space applications over many years (more than forty years) and production mechanisms of single-event effects (SEE) in semiconductor devices by protons or heavy ions well apprehended, characterized and modeled [6]. In a similar way for avionic applications, the interaction of atmospheric neutrons with electronics has been identified as the major source of SEE [7]. For the most recent deca-nanometers technologies, the impact of other atmospheric particles produced in nuclear cascade showers on circuits has been clearly demonstrated (protons [8-9]) or is still under exploration for some exotic particles (pions and charged muons [10-14]).

With respect to such high-altitude atmospheric environments, the situation at ground level is slightly different. Of course, atmospheric neutrons are always the primary particles but, with a flux approximately divided by a factor ~300 at sea-level with respect to the flux at avionics altitudes, the Soft-Error Rate (SER) of circuits can be now affected by an additional source of radiation, usually neglected because completely screened by

neutrons in avionics: the alpha particles generated from traces of radioactive contaminants in CMOS process or packaging materials [1,15]. As a consequence of these multiple sources of radiation, the accurate modeling and simulation of the SER of circuits at ground level is rather a complex task because one can clearly separate the contribution to SER of atmospheric particles (the external constraint) from the one due to natural alpha-particle emitters present as contaminants in circuit materials (the internal constraint).

Modeling and simulating the effects of ionizing radiation has long been used for better understanding the radiation effects on the operation of devices and circuits [16-19]. In the last two decades, due to substantial progress in simulation codes and computer performances which reduce computation times, simulation reached an increased interest. Due to its predictive capability, simulation offers the possibility to reduce radiation experiments and to test hypothetical devices or conditions, which are not feasible (or not easily measurable) by experiments. Physically-based numerical simulation at device-level presently becomes an indispensable tool for the analysis of new phenomena specific to short-channel devices and for the study of radiation effects in new device architectures for which experimental investigation is still limited [19]. In these cases, numerical simulation is an ideal investigation tool for providing physical insights and predicting the operation of future devices expected for the end of the microelectronic roadmap. Last but not least, the understanding of the soft error mechanisms in such devices and the prediction of their occurrence under a given radiation environment are of fundamental importance for certain applications requiring a very high level of reliability and dependability [1].

In this framework, this chapter describes in details a complete general purpose simulation platform we have developed these last years for the numerical evaluation of the sensitivity of advanced semiconductor memories (static RAMs) subjected to natural radiation at ground level. The physical modeling approach we developed as well as the object-oriented programming implementation are very general and can be used to simulate both external or internal radiation constraints, i.e. the bombardment of the memory circuit by heavy-ions, neutrons, protons, muons, etc. or the generation of alpha-particles inside the circuit materials due to the presence of traces of radioactive contaminants.

The chapter is organized as follows. After introducing the natural radiation environment at ground level and the different types of radiation constraints in section 2 and the basic mechanisms of single-event effects on microelectronic devices in section 3, section 4 will present in details the different modules of our multi-scale and multi-physics numerical simulation chain, including some important precisions related to the modeling of the circuit architecture, the generation of particles mimicked a given radiation environment and the physical-based modeling of the circuit/cell electrical response. Finally, in section 5, we will illustrate various capabilities of our code to estimate the soft-error rate of different SRAM circuits representative of advanced technological nodes.

2. Natural radiation at ground level

As briefly stated in the introduction, natural radiation that causes soft error in digital circuits may come from various sources. At ground level, one can distinguish two major sources of radiation described in the following: i) the atmospheric radiation environment and ii) the telluric radiation sources,.

2.1. Atmospheric radiation environment

The cascades of elementary particles and electromagnetic radiation are produced in the Earth's atmosphere when a primary cosmic ray (of extraterrestrial origin) enters the atmosphere [20]. The term cascade means that the incident particle (generally a proton, a nucleus, an electron or a photon) strikes a molecule in the air so as to produce many high energy secondary particles (photons, electrons, hadrons, nuclei) which in turn create more particles, and so on.

Among all these produced secondary particles, neutrons represent the most important part of the natural radiation constraint at ground level susceptible to impact electronics. Because neutrons are not charged, they are very invasive and can penetrate deeply in circuit materials. They can interact via nuclear reactions with the atoms of the target materials and create (via elastic or inelastic processes) secondary ionizing particles. This mechanism is called "indirect ionization" and is potentially an important source of errors induced in electronic components. One generally distinguishes thermal neutrons (interacting with ^{10}B isotopes potentially present in circuit materials, but progressively removed from technological processes [5]) and high-energy atmospheric neutrons (up to the GeV scale). Figure 1 (top) shows the typical energy distribution of atmospheric neutrons, ranging from thermal energies to 1 GeV, as measured by Goldhagen et al. [21] using a Bonner multi-sphere spectrometer at the reference location (New-York City, NYC). The integration of this spectrum, also shown in Figure 1 (bottom), gives the total neutron flux expressed in neutrons per square centimeter and per hour: this flux is equal to 7.6 n/cm^2/h for the lower part (thermal and epithermal neutrons below 1 eV), 16 n/cm^2/h for the intermediate part (between 1 eV and 1 MeV) and 20 n/cm^2/h for the upper part (high energy neutrons above 1 MeV).

Atmospheric muons also represent an important part of the natural radiation constraint at ground level [20]. Muons belong to the meson or "hard" component in the atmospheric cosmic ray cascades and are the products of the decay of charged pions (instable particles with a short lifetime of 26 ns) via the weak interaction. They are easily able to penetrate the atmosphere down to sea level and they constitute the only secondary cosmic radiation able to penetrate significant depths underground. In spite of a lifetime of about 2.2 μs, most of them survive to sea level and constitute the most preponderant charged particles at sea level. But despite this abundance, muons interact extremely few with matter, excepted at low energies by direct ionization (see subsection 5.3).

In contrast and while strongly interacting with matter, pions are not enough abundant at ground level to induce significant effects in components. Furthermore, for modern

technologies, the small amount of electrons and gamma-rays having very low energy are not able to disrupt electronics.

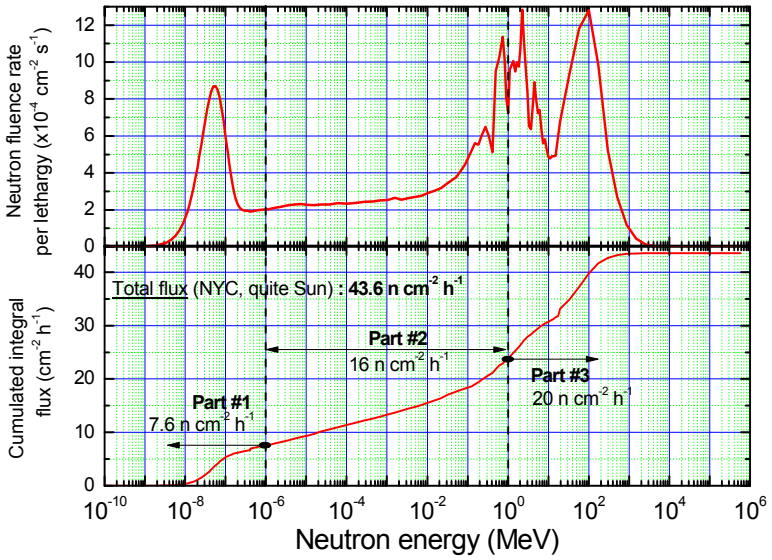

Figure 1. Top: Reference atmospheric neutron spectrum measured on the roof of the IBM Watson Research Center main building [21]. Numerical data courtesy from Paul Goldhagen (U.S. Department of Homeland Security). Bottom: Cumulated integral flux corresponding to the above spectrum. The total neutron flux is 43.6 neutrons per cm^2 and per hour.

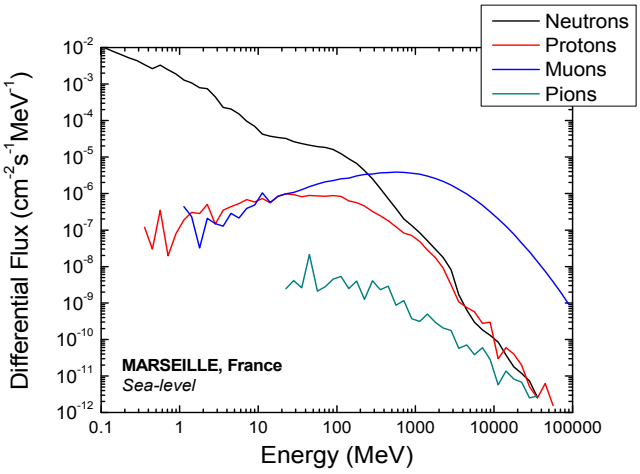

Figure 2. High energy (> 0.1 MeV) differential flux for atmospheric neutrons, protons, muons and pions at ground level. Data computed using the Qinetic Atmospheric Radiation Model [22-23] for Marseille, France (Latitude 43.18' N, Longitude 5.22' E, sea-level).

Finally, protons, although they interact with silicon as neutrons above a few tens of MeV, are one hundred times less numerous than the latter at ground level. Their low abundance allows us to consider their impact as negligible compared with that of neutrons, except at low energies (< 1 MeV) for which certain advanced technologies show an exacerbated sensitivity due to charge deposition by direct ionization.

Figure 2 shows a typical energy distribution of the differential flux for atmospheric neutrons, protons, muons and pions at ground level. Such a collection of spectra, characteristic of a given location (latitude, longitude and elevation), constitute a set of input data of primary importance for any simulation code dedicated to the evaluation of the soft error rate induced by the atmospheric radiation environment (see section 4).

2.2. Telluric radiation sources

Natural radioisotopes contained in the Earth's crust are the principal natural sources of α, β and γ radioactivity but only the alpha-particle emitters present a reliability concern in microelectronics. Beta and gamma processes are indeed not able to deposit a high enough amount of energy susceptible to significantly impact the microelectronic circuit operation. The presence of alpha-particle emitters in electronic devices can be classified as materials that are naturally radioactive (they contain a fraction of radioactive nuclei) or materials that contain residual trace of radioactive impurities [24]. Currently, several types of alpha-particle emitters have been identified at wafer, packaging and interconnection levels, including lead in solder bumps, uranium and thorium in silicon wafers and in molding compounds, more recently hafnium in new high-κ gate and platinum in silicide materials.

Considering the activity of radioisotopes in the calculation of the soft error rate of a circuit thus requires to accurately modeling the alpha-particle source mimicking the presence of these alpha-particle emitters in the circuit materials. For example, considering traces of uranium in a given material (silicon for example) requires to take into account the complete uranium disintegration chain composed of 14 daughter nuclei with 8 alpha-particle emitters. Energies of the alpha-particle are ranging from 4.20 to 7.68 MeV; their corresponding ranges

	$T_{1/2}$ (s)	Alpha Energy (MeV)	Range in Si (µm)	Corresponding initial LET (MeV/(mg/cm²))
^{238}U	$1.40\times10^{+17}$	4.19	18.95	0.677
^{234}U	$7.76\times10^{+12}$	4.68	22.17	0.634
^{230}Th	$2.38\times10^{+12}$	4.58	21.49	0.642
^{226}Ra	$5.05\times10^{+10}$	4.77	22.78	0.627
^{222}Rn	$3.30\times10^{+05}$	5.49	27.94	0.575
^{218}Po	$1.86\times10^{+02}$	6.00	31.86	0.545
^{214}Po	1.64×10^{-04}	7.68	46.22	0.468
^{210}Po	$1.20\times10^{+07}$	5.31	26.61	0.588

Table 1. Main characteristics (half-life, mean energy, range in silicon and initial linear energy transfer of the emitted alpha-particle) of the eight alpha-emitters of the disintegration chain of ^{238}U [25].

in silicon vary from 19 to 46 μm and their initial Linear Energy Transfer (LET) from 0.47 to 0.68 MeV/(mg/cm²), as summarized in Table 1.

3. Basic mechanisms of single-event effects on microelectronic devices

In this section, we briefly summarize the physical mechanisms related to the production of SEE in microelectronic devices by a charged particle. This general scheme can be applied to all particles able to directly deposit an electrical charge along their track (heavy ions, alpha-particles, low energy protons and low energy muons). As we already mentioned for neutrons, the ionization is indirect since neutron is a neutral particle but it can induce charged particles (recoil atoms or secondary particle) by nuclear reaction with the atoms of the target material. The following scenario can thus be applied separately to all secondary charged particles produced by the neutron.

Considering a single charged particle, the passage of this particle through a portion of a microelectronic circuit consists in three main successive steps: (1) the charge deposition by the energetic particle striking the sensitive region, (2) the transport of the released charge into the device and (3) the charge collection in the sensitive region of the device. Figure 3 schematically shows these successive steps in the case of the passage of the energetic charged particle through a reverse-biased n^+/p junction. In the following we succinctly describe these different mechanisms, for a detailed presentation we invite the reader to consult references [5][16-19].

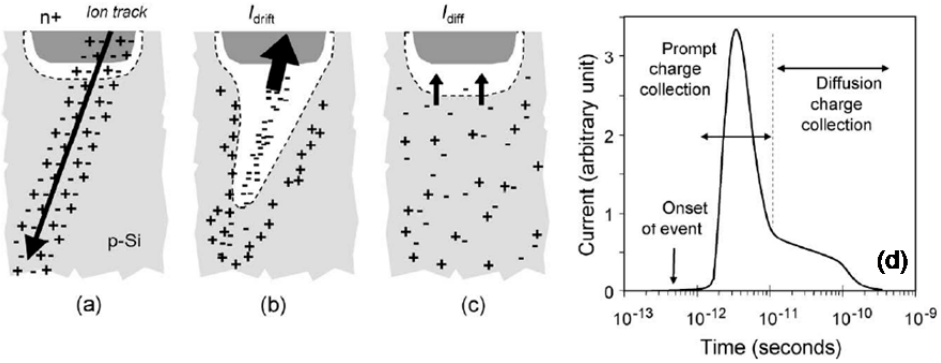

Figure 3. Charge generation, transport and collections phases in a reverse-biased junction and the resultant current pulse caused by the passage of an energetic charged particle. After Baumann [5]. © 2005 Institute of Electrical and Electronics Engineers Inc., reproduced with permission.

Charge deposition (or generation): When the particle strikes the device, an electrical charge along the particle track can be deposited by direct ionization of the target material. This direct ionization is mainly produced by inelastic interactions and transmits a large amount of energy to the electrons of the struck atoms. These electrons produce a cascade of secondary electrons which thermalize and create electron-hole pairs along the particle path [Figure 3(a)]. In a semiconductor or insulator, a large amount of the deposited energy is thus

converted into electron-hole pairs, the remaining energy being converted into heat and a very small quantity in atoms displacement. It was experimentally shown that the energy necessary for the creation of an electron-hole pair depends on the material bandgap. In a Silicon substrate, one electron-hole pair is produced for every 3.6 eV of energy lost by the particle.

As already mentioned, neutrons of the terrestrial environment do not interact directly with target material since they do not ionize the matter on their passage. However, the products resulting from a nuclear reaction can deposit energy along their traces, in the same manner as that of direct ionization. Since the creation of the column of electron-hole pairs of these secondary particles is similar to that of ions, the same models and concepts can be used.

Charge transport: When a charge column is created in the semiconductor by an ionizing particle, the released carriers are quickly transported and collected by elementary structures (e.g. p-n junctions). The transport of charge relies on two main mechanisms [Figures 3(b) and 3(c)]: the charge drift in regions with an electric field and the charge diffusion in neutral zones. The deposited charges can also recombine with other mobile carriers existing in the lattice.

Charge collection: The charges transported in the device induce a parasitic current transient [Figure 3(d)], which could induce disturbances in the device and associated circuits. The devices most sensitive to ionizing particle strikes are generally devices containing reversely-biased p-n junctions, because the strong electric field existing in the depletion region of the p-n junction allows a very efficient collection of the deposited charge. The effects of ionizing radiation are different according to the intensity of the current transient, as well as the number of impacted circuit nodes. If the current is sufficiently important, it can induce a permanent damage on gate insulators (gate rupture, SEGR) or the latch-up (SEL) of the device. In usual low power circuits, the transient current may generally induce only an eventual change of the logical state (cell upset).

4. The TIARA-G4 Monte Carlo simulation code

This section describes in details the TIARA-G4 code developed these last years conjointly at Aix-Marseille University (IM2NP laboratory) and at STMicroelectronics (Central R&D, Crolles). TIARA-G4 is a general-purpose Monte Carlo simulation code written in C++ and fully based on the Geant4 toolkit for modeling the interaction of Geant4 particles (including neutrons, protons, muons, alpha-particles and heavy ions) with various architectures of electronic circuits. TIARA stands for Tool Suite for Radiation Reliability Assessment. The primary ambition of TIARA is to embed in a unique simulation platform the state-of-the-art knowledge and methodology of SER evaluation.

The initial version of TIARA [26-27] was a standalone C++ native code dynamically linked with IC CAD flow through the coupling with a SPICE solver. The code has been developed such that the addition of new radiation environments, physical models or new circuit architecture should be quite simple. On one hand, this first version was able to treat the

transport and energy deposition of charged particles (heavy ions and alpha particles) without the need for a nuclear code as Geant4 [28]; only SRIM [29] tables were used as input files to compute the transport of the particles in silicon and in a simplified Back-End-Of-Line (BEOL) structure reduced to a single layer. On the other hand, for neutrons, it used separate databases compiled using a specific Geant4 application to generate nuclear events in the simulation flow resulting from the interactions of incident neutrons with the circuit.

The new version of TIARA, described here, is called TIARA-G4, in reference to the fact that it is totally rewritten in C++ using Geant4 classes and libraries and compiled as a full Geant4 application [28]. The main improvement of TIARA-G4 with respect to the first version of the code comes precisely from this transformation of the code in a Geant4 application, allowing the use of Geant4 classes for the description of the circuit geometry and materials (now including the true BEOL structure) and the integration of the particle transport and tracking directly in the simulation flow, without the need of external databases or additional files. Figure 4 shows a schematics of the TIARA-G4 simulation flow structured in several independent modules. In the following, we present the content of the main modules of the code and illustrate (also in Section 5) their capabilities for the soft error rate evaluation of different SRAM CMOS bulk circuits (65 nm and 40 nm technologies) subjected to natural radiation at ground level.

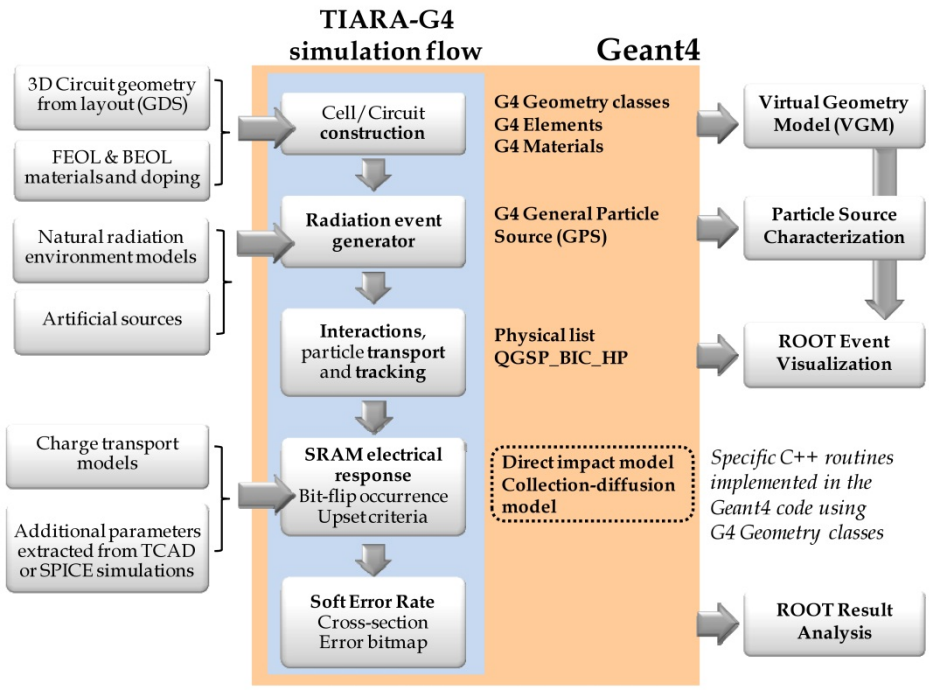

Figure 4. Schematics of the TIARA-G4 simulation flow showing the different code inputs and outputs and the links with Geant4 classes, libraries, models or external modules and visualization tools.

4.1. Circuit architecture construction module

The first step of the TIARA-G4 simulation is to construct a model of the simulated circuit from Geant4 geometry classes and libraries of elements and materials. In the framework of Geant4, the circuit under simulation is considered as the "particle detector". The structure creation in TIARA is based on 3D circuit geometry information extracted from GDS formatted data classically used in the Computer-Aided Design (CAD) flow of semiconductor circuit manufacturing. To perform such an extraction from the GDS layout description, a separate tool has been developed [30]. It parses the GDS file, obtains coordinate points of CAD layers and using geometrical computations tracks the positions and dimensions of the transistor active areas, cell dimensions, p-type and n-type and Back-End-Of-Line (BEOL) stack geometry. Based on this information and additional data concerning the depth of the wells, junctions, STI regions (obtained from TCAD or SIMS measurements) and BEOL layer composition, TIARA creates a 3D structure of the elementary memory cell and, by repetition, of the complete portion of the simulated circuit. The real 3D geometry is simplified since it is essentially based on the juxtaposition of boxes of different dimensions, each box being associated to a given material (silicon, insulator, metal, etc.) or doped semiconductor (p-type, n-type).

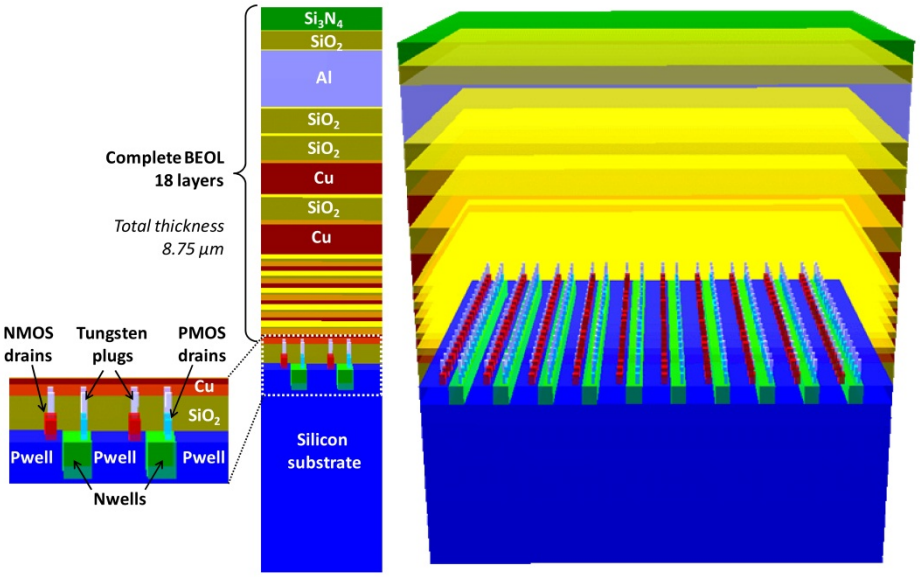

Figure 5. Left and Center**:** ROOT screenshots illustrating the geometry of the complete 65 nm SRAM architecture considered in TIARA-G4 simulation. Right: 3D perspective view of a 10×20 SRAM cell array covered with the BEOL.

Figure 5 (left) illustrates the geometry of a complete 65 nm SRAM architecture considered in TIARA-G4 simulation. Sensitive Pmos and Nmos drains regions are connected to the first metal layer (Cu) of the BEOL stack with tungsten plugs. The BEOL structure is composed of 18 uniform stacked layers with exact compositions and thicknesses. The 3D perspective

view of a 10×20 SRAM cell array covered with the BEOL is shown in Figure 5 (right). For better visibility, BEOL layers have been rendered semi-transparent in this illustration.

4.2. Radiation event generator

To numerically generate the particles with the spectral, spatial and angular distributions mimicking all the characteristics of the natural background, as introduced and defined in section 2, we use the G4 General Particle Source (GPS) [31] which is part of the Geant4 distribution. The module allows the user to define all the source parameters, in particular the energy of the emitted particles from a given energy distribution defined in a separate input file.

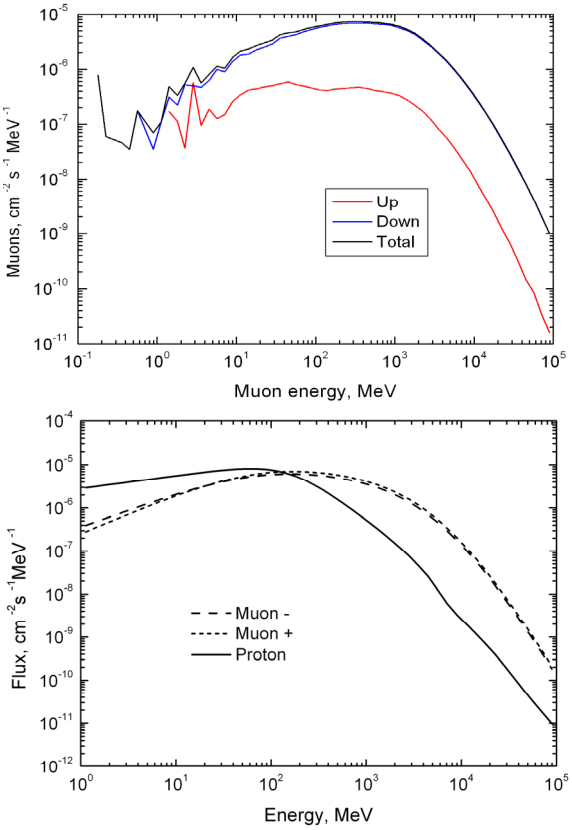

Figure 6. Differential fluxes of atmospheric muons given by the QARM (top) [22-23] and PARMA (bottom) [33-34] models at the location of the Altitude SEE Test European Platform (ASTEP, latitude North 44° 38′ 02′′, longitude East 5° 54′ 26′′, altitude 2555 m, see www.astep.eu). The atmospheric proton spectrum calculated with the PARMA model is also plotted (bottom).

For atmospheric particles, the energy distributions of neutrons, protons, pions and muons reaching the ground level are available in the literature or on the web as functions of latitude,

longitude and altitude. They are obtained from direct measurements and/or from Monte Carlo simulations. For the neutron flux, we use the experimental atmospheric spectrum presented in Figure 1, which is actually the reference curve (for high-energy neutrons above 1 MeV) for the JEDEC Standard JESD89A [32]. For the other atmospheric particles (mainly muons and protons), we adopted the QinetiQ Atmospheric Radiation Model (QARM) [22-23] and the PARMA model [33-34], which are specifically developed for prediction of the radiation in the atmosphere for a given location and date. Figure 6 shows the differential fluxes of atmospheric muons (resp. protons) given by these two models (resp. by PARMA).

Another important issue in Monte-Carlo simulation is the strong zenith angular dependence of atmospheric showers. To make our Geant4 GPS primary particle sources more realistic, we introduce in simulations the angular dependence of the primary flux intensity in the form $I(\theta) \sim \cos^n(\theta)$ where θ is the zenith angle and n a parameter fixed to n=3.5 for neutrons [35], and for muons n=2 [36].

For the simulation of alpha-particle emitters present in the IC materials, we directly generate in the code the random positions and emission directions with uniform probability densities for each daughter element of the considered decay chain (uranium or thorium).

4.3. Interaction, transport and tracking module

Once an incident particle has been numerically generated with the radiation event generator, the Geant4 simulation flow computes the interactions of this particle with the target (the simulated circuit) and transports step-by-step the particle and all the secondary particles eventually produced inside the world volume (the largest volume containing, with some margins, all other volumes contained in the circuit geometry). The transport of each particle occurs until the particle loses its kinetic energy to zero, disappears by an interaction or comes to the end of the world volume.

The G4ProcessManager class contains the list of processes that a particle can undertake. A physical process describes how particles interact with materials. The list of physical processes employed in our simulations is based on the physics lists QGSP_BIC_HP [37], one of the standard Geant4 list covering the energy range of particles interacting in low- to medium-energy ranges. This list uses binary cascade, precompound and various de-excitation models for hadrons standard EM, with high precision neutron model used for neutrons below 20 MeV. This list is generally used for simulations in the fields of radiation protection, shielding and medical applications.

Geant4 provides a way for the user to access the transportation process and to obtain the simulation results at the beginning and end of transportation, at the end of each stepping in transportation and at the time when the particle is going into a given sensitive volume of the circuit. Tables 2 and 3 shows two intermediate output results of TIARA-G4 respectively describing a particle interaction event (Table 2, nuclear inelastic event with a silicon atom of the p-type silicon substrate of the circuit, see Figure 5) and the tracking of two secondary particles impact different sensitive volumes of the circuit (Table 3). All these output data are

saved as text files during the simulation and can be used later for event visualization or post-processing. Finally, Figure 7 illustrates the visualization of an interaction event (here a negative muon capture by a silicon atom) using ROOT [38]. Such a 3D perspective view is computed using a dedicated ROOT script which directly imports geometry and event data from a collection of files saved on the machine hard disk during simulation.

Event #2359425
Incident particle: neutron
Energy (MeV): 5.664161e+01
Physical process: NeutronInelastic
Volume name: P-substrate
Reaction vextex positions (x,y,z): -5.656377e+00 -1.377065e+00 -5.347320e+00

Number of secondary particles produced: 5

Particle	Energy (MeV)	Px	Py	Pz
Alpha	3.197153e+01	6.097439e-01	-5.070998e-01	6.091488e-01
Neutron	1.697277e+00	-9.311596e-01	3.551987e-01	8.231417e-02
Gamma	9.051714e+00	3.281911e-01	-6.857286e-02	9.421191e-01
Gamma	1.377447e+00	2.331650e-01	8.485282e-01	4.750095e-01
Mg24[0.0]	2.554443e+00	-7.370831e-01	6.733902e-01	5.704476e-02

Table 2. Table 2. Example of a TIARA-G4 output in case of particle interaction with the target (circuit). The present example describes a neutron inelastic process (energy of the incident neutron of 56.64 MeV) with a silicon atom of the p-type substrate of the circuit described in Figure 4. This nuclear reaction produces 5 secondary particles at the reaction vertex position; for each produced particle, the particle energy and the three components of the normalized particle momentum (Px, Py, Pz) are indicated.

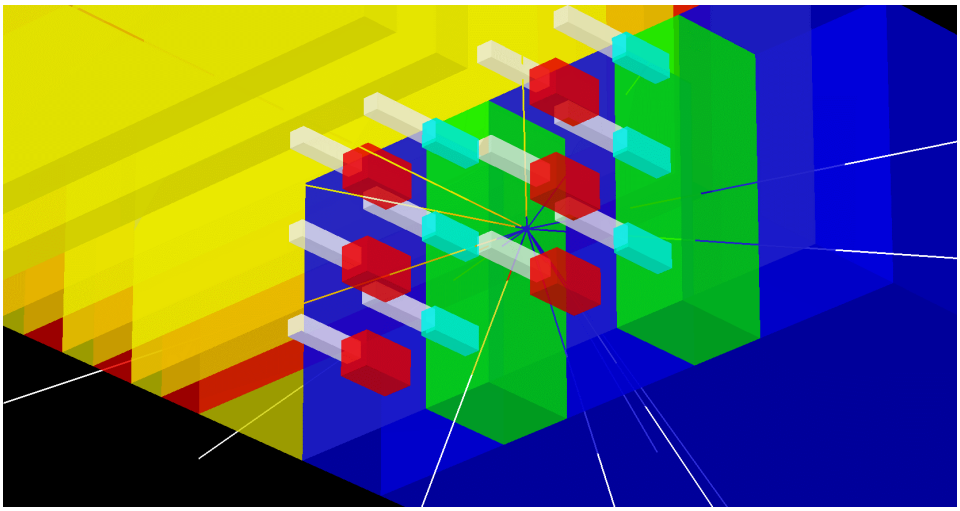

Figure 7. TIARA-G4 screenshot under ROOT visualization tool showing a part of the memory circuit (65 nm SRAM) subjected to a negative muon irradiation. The resulting interaction shown here is a muon capture by a silicon atom in the active circuit region (Pwell) produced a shower of ten secondary particles.

```
Event #5477703
EventStepData.size: 5
-----------------------------------------------------
StepData object #0    ParticleName: Al28[0.0]
VolumeName: Psub #0
initPoint/um: (-2.234447e+00,-1.624657e+00,-8.960758e-01)
postPoint/um: (-2.239293e+00,-1.703238e+00,-8.400000e-01)
EnergyDep/MeV: 7.491555e-02
-----------------------------------------------------
StepData object #1    ParticleName: Al28[0.0]
VolumeName: Pwell #8
initPoint/um: (-2.239293e+00,-1.703238e+00,-8.400000e-01)
postPoint/um: (-2.233404e+00,-2.258219e+00,-3.596903e-01)
EnergyDep/MeV: 4.304428e-01
-----------------------------------------------------
StepData object #2    ParticleName: proton
VolumeName: Psub #0
initPoint/um: (-2.234447e+00,-1.624657e+00,-8.960758e-01)
postPoint/um: (-2.230874e+00,-1.572415e+00,-8.400000e-01)
EnergyDep/MeV: 2.421962e-04
-----------------------------------------------------
StepData object #3    ParticleName: proton
VolumeName: Pwell #8
initPoint/um: (-2.230874e+00,-1.572415e+00,-8.400000e-01)
postPoint/um: (-2.196440e+00,-1.069293e+00,-3.000000e-01)
EnergyDep/MeV: 2.737365e-03
-----------------------------------------------------
StepData object #4ParticleName: proton
VolumeName: Nmos #168
initPoint/um: (-2.181468e+00,-8.495000e-01,-6.405073e-02)
postPoint/um: (-2.177411e+00,-7.898294e-01,0.000000e+00)
EnergyDep/MeV: 2.871799e-04
```

Table 3. Example of the tracking of two secondary particles (^{28}Al and proton) impacting different sensitive volumes (Psub, Pwell and Nmos) of the SRAM circuit. For each particle and each impacted sensitive volume, the (x, y, z) coordinates of the entry and exit points of the particle in this volume are indicated and also the energy deposited by the particle in this same volume.

4.4. SRAM electrical response module

We detail in this section the model used to calculate the electrical response of the SRAM circuit subjected to the irradiation. Starting a simulation sequence when a primary particle emitted by the particle source enters in the world volume, we already mentioned that Geant4 computes the interactions of this particle with the circuit and transports step-by-step the particle and all the secondary particles (eventually produced) until all these particles loss their kinetic energy to zero, disappear by interaction or come to the end of the world volume.

At the end of the sequence,TIARA-G4 examines the tracks of all the charged particles involved in this simulation step (including eventually the track of the incident primary particle if it is charged) and determine the complete list of the different silicon volumes (drains, Pwells, Nwells, substrates, etc.) traversed by these particles. Two very general

cases can be distinguished from this pure geometrical analysis, as schematically shown in Figure 8:

1. A single or several charged particles directly pass through a sensitive drain volume. In this case, TIARA-G4 directly evaluates from Geant4 data the total energy deposited by these particles in the drain (ΔE), converts this value into a number of generated electron-hole pairs ($Q_{dep} = \Delta E/3.6$ eV for bulk silicon) and finally compares this value with the critical charge value ($Q_{crit,P}$ for Pmos, $Q_{crit,N}$ for Nmos) of the simulated technology. If $Q_{dep} > Q_{crit}$, the memory cell is considered to be upset, in the contrary case, the electrical state of the cell is not changed [19].
2. A single or several charged particles impact one or several Nwell, Pwell and/or the silicon substrate. In this case, TIARA-G4 evaluates for each sensitive drain located in the impacted Nwell(s) (for Pmos) or Pwell(s) and substrate (for Nmos) the transient current I(t) resulting from the diffusion of carriers in excess in these regions and the collection of the charge by the sensitive nodes (see also Figure 9). Such calculations are performed using the "diffusion-collection model" detailed in the following. Until the I(t) characteristic is computed for all the considered sensitive drains, TIARA-G4 applies the "I_{max}-t_{max}" criterion, also described below, to determine if the corresponding memory cell is upset or not.

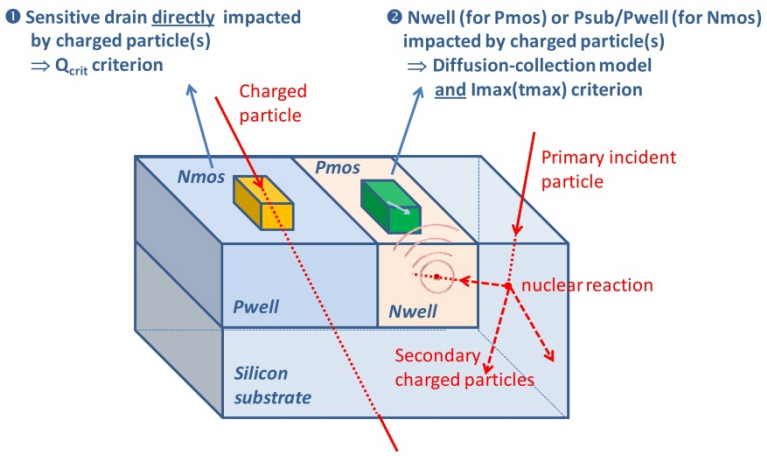

Figure 8. Schematics of the different cases envisaged in TIARA-G4 for the evaluation of cell upset in the simulated SRAM circuit.

In the diffusion-collection model [39-40], the energy lost by a charged particle in silicon along its track is converted in a succession of elementary carrier densities δQ. The model then assumes that the behavior of these quasi-point charges is governed by a pure 3D spherical diffusion law:

$$\frac{\partial n}{\partial t} = D \cdot \Delta n \tag{1}$$

where n is the carrier density in excess generated in the silicon and D is an ambipolar diffusion coefficient.

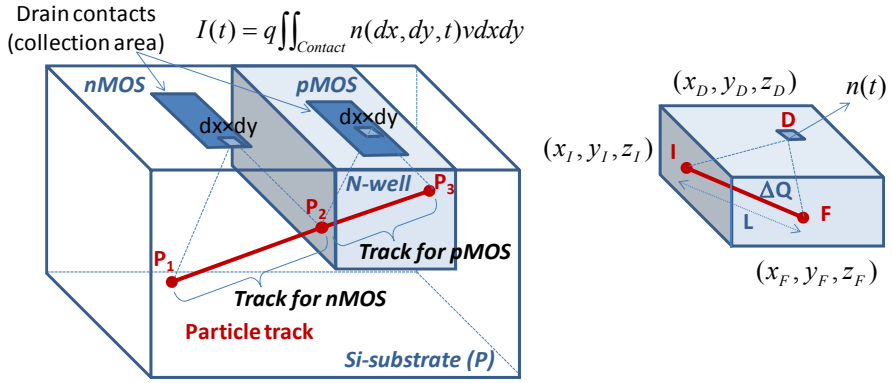

Figure 9. Left: Schematics of the "diffusion-collection model" used to compute the transient current I(t) resulting from the 3D spherical diffusion and then from the collection by a given reverse-biased drain of the charge in excess generated along a charged particle track. Right: Definition of the different points in Cartesian coordinates used to numerically evaluate n(t).

The temporal and spatial concentration n(r,t) resulting from the diffusion of a quasi-ponctual charge δQ in the silicon at the distance r from this charge is thus described by the following equation:

$$n(r,t) = \frac{\delta Q}{\sqrt[3]{4\pi Dt}} \times \exp\left(-\frac{r^2}{4Dt} - \frac{t}{\tau}\right) \tag{2}$$

where τ is the carrier lifetime, r is the distance from the element δQ, and t is the time.

In the present implementation of the diffusion-collection model, δQ is directly evaluated from Geant4 data, considering the energy lost by the particle in a given geometry volume. Figure 9 (right) illustrates the general case of a given volume impacted by a particle. The particle enters the volume in point I and exits in point F. Because drain and well volumes have reduced dimensions (typically expressed in tenths of a micron), the electrical charge δQ deposited per elementary length dl can be approximated by $Q_{dep} \times dl / L$ where L is the length of the segment IF. Considering the Cartesian coordinates of the geometrical points I, F and D defined on Figure 8, the total collected charge at point D due to the contribution of the complete segment IF can be analytically evaluated from the following expression:

$$n(t) = \frac{\delta Q / q}{8\pi DtL} \times \exp\left(-\frac{l_0^2}{4Dt} - \frac{t}{\tau}\right) \times \exp\left(-\frac{K^2}{L^2 4Dt}\right) \times \left\{erf\left[\frac{1}{2\sqrt{Dt}}\left(L + \frac{K}{L}\right)\right] - erf\left[\frac{K}{2L\sqrt{Dt}}\right]\right\} \tag{3}$$

where quantities L, l_0 and K are defined from the Cartesian coordinates of points I, F and D:

$$\begin{cases} L = \sqrt{\left(x_F - x_I\right)^2 + \left(y_F - y_I\right)^2 + \left(z_F - z_I\right)^2} \\ l_0^2 = \left(x_D - x_I\right)^2 + \left(y_D - y_I\right)^2 + \left(z_D - z_I\right)^2 \\ K = \left(x_I - x_D\right)\left(x_F - x_I\right) + \left(y_I - y_D\right)\left(y_F - y_I\right) + \left(z_I - z_D\right)\left(z_F - z_I\right) \end{cases} \quad (4)$$

The total electrical charge from the particle track collected at the level of a sensitive drain electrode is obtained by integrating Eq. (3) on the total drain surface, as illustrated in Figure 9. Then, the charge is converted into a current by multiplying n(t) by the elementary charge and by the average collection velocity via space charge region of the reverse-biased drain:

$$I(t) = q\iint_{Contact} n(t) \cdot v \cdot dxdy \quad (5)$$

Once the I(t) characteristic has been computed for all drains of the sensitive transistors in the SRAM cell matrix, TIARA-G4 applies the I_{max}-t_{max} criterion [26] to determine the cell upsets. This criterion is separately obtained from TIARA-G4 simulation and requires the combination of TCAD and PSICE analysis. The calculated $I_{max}(t_{max})$ characteristic delimitates two current-time domains, as illustrated in Figure 10. If the transient current peak is located above this curve, an upset occurs; in the contrary case the extracted transient current from the sensitive node is not able to sufficiently disturb the electrical state of the bi-stable flip-flop and consequently to upset the memory point.

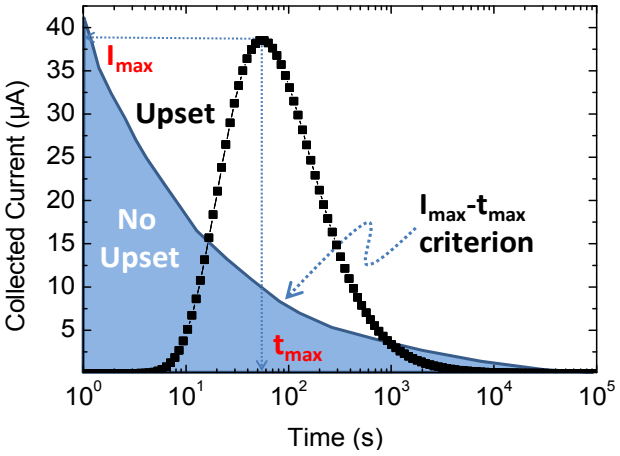

Figure 10. Example of a transient current characteristic superimposed to the I_{max}-t_{max} upset criterion. The transient current has been calculated from the "diffusion-collection model" for a ^{24}Mg particle (10 MeV) which perpendicularly impacts a Pwell at the distance of 0.25 μm from the Nmos drain contact.

4.5. Soft error rate calculation module

At the end of the simulation flow, the last module of the TIARA-G4 code evaluates the Soft Error Rate (SER) of the SRAM circuit from the following expression [32]:

$$SER[\text{FIT/Mbit}] = \frac{1024 \times 1024}{CellNum} \times \frac{IntFlux[cm^{-2}]}{NumPart} \times L_X[\text{cm}] \times L_Y[\text{cm}] \times 10^9 \times TotalUpsetNum \quad (6)$$

where TotalUpsetNum is the total number of cell upsets obtained during the simulation, CellNum is the number of memory cells of the simulated circuit, L_X and L_Y are the circuit dimensions (in cm), NumPart is the total number of primary particles incident on the simulated circuit and IntFlux is the integral flux (cm^{-2}) of the particle source used to generate the incident particles. For example, considering the atmospheric neutron spectrum of Figure 1, IntFLux = 7.6 n/cm^2 for Part #1, 16 n/cm^2 for Part #2 and 20 n/cm^2 for Part #3 of the spectrum.

5. Simulation results

In this last section, the capabilities of the TIARA-G4 code are illustrated though a few dedicated studies on the simulation of 65 nm or 40 nm CMOS bulk SRAM circuits subjected to different sources of atmospheric particles. These three examples are independent and respectively concern: i) the impact of thermal and low energy neutrons on a 40 nm SRAM circuit; ii) the SER estimation of a 65 nm SRAM under high energy atmospheric neutrons and iii) the effects of low-energy muons on the same 65 nm circuit.

5.1. Impact of thermal and low energy neutrons on a 40 nm SRAM circuit

Since the 80's, the interaction of cosmic ray induced thermal neutrons with the ^{10}B isotope of the boron has been identified as a major source of soft errors in electronic circuits [41]. ^{10}B only represents 19.9% abundance of natural boron but the very large cross section of the $^{10}B(n,\alpha)7Li$ reaction at thermal energies combined with the highly ionizing character and the range in silicon of the two nuclei produced by this fission reaction (one lithium nucleus and one alpha particle) can easily explain the danger of ^{10}B when it is present in elevated concentration in close proximity to the sensitive regions of integrated devices [41]. Modern semiconductor processes have thus completely eliminated the presence of ^{10}B in Borophosphosilicate glasses (BPSG) used in the back-end-of-line (or outright the use of the BPSG itself), considered as the principal reservoir of ^{10}B and the dominant source of boron fission in circuits. However, ^{10}B remains present at silicon level, since bulk substrate doping and source/drain implantation are not selective in isotope and continue to use natural boron [41-42]. The issue of thermal neutron sensitivity to current technologies is still relevant and remains open, in particular for ultra-scaled technologies in the natural terrestrial environment at ground level. Recent work demonstrated a substantial SER sensitivity with neutron energies for many SRAM circuits in the 0.25 μm-45 nm technology range [43-44].

Using the new TIARA-G4 code, we propose here to explore the question of thermal and low energy neutron-induced soft errors in state-of-the-art 40 nm SRAMs. Such a study can be only conducted with a code taking into account the real geometry at silicon level, including the silicon doping with natural boron in p-type regions containing 19.9% of ^{10}B. We thus constructed a 40 nm SRAM matrix with exact doping levels at the level of Pwells ([B] = 10^{16} cm^{-3}) and Pmos drains ([B] = 3×10^{20} cm^{-3}).

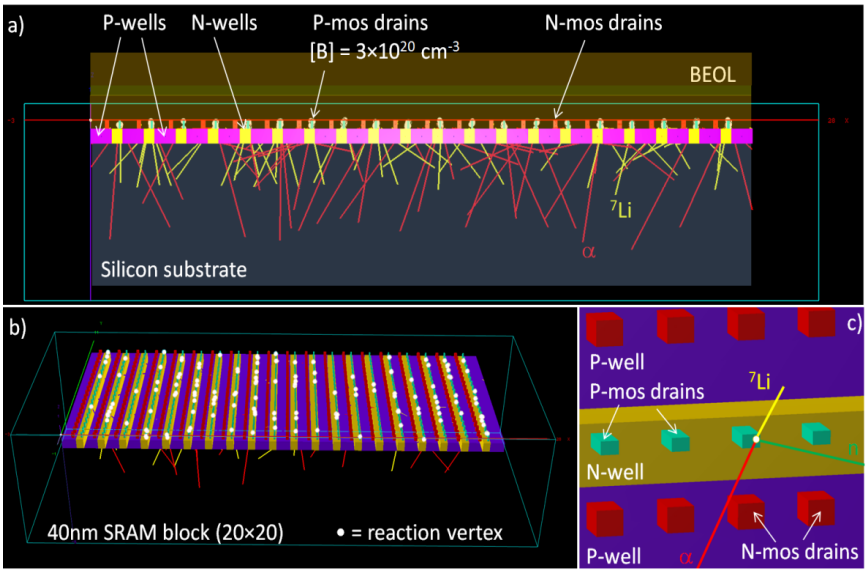

Figure 11. TIARA-G4 screenshots under ROOT illustrating the results of 2×10^9 thermal neutrons incident on the 40 nm single-port SRAM (20×20 memory cell block). White points correspond to the reaction vertex (only localized in the Pmos drain volumes); colored segments to the trajectories of the secondary ions produced (red for alpha, yellow for ^{7}Li). For clarity, BEOL and substrate have been removed from the perspective view in b). c) Detail a ^{10}B fission reaction occurring in the volume of a Pmos drain (note that the alpha-particle and the lithium nucleus are emitted in opposite directions to conserve momentum).

Figure 11 illustrates the simulation results obtained on a 20×20 SRAM matrix. This circuit was irradiated with thermal and low energy neutrons generated by the Geant4 GPS source considering Part #1 of the reference atmospheric spectrum shown in Figure 1. In order to obtain a sufficient event statistic (interaction events are relatively rare), we pushed the number of incident particles up to 2×10^9 thermal neutrons. A total 116 single bit upsets (SBU) and 24 multiple celle upsets (MCU) have been detected: they are exclusively the result of ^{10}B fission events localized in the drain volumes of the Pmos transistors (see Figure 11(b), the vertex of the reactions are indicated by the white dots).

Figure 12 shows that both the SER value and the event multiplicity distributions are in excellent agreement with experimental data performed at the LLB facility, located at CEA Saclay, France [45]. The experiment was conducted on the G3-2 beam line under a thermal neutron flux reduced to 7.88×10^8 n/cm^2/s (beam surface area of 25×50 mm2, neutron energies in the range 1.8-10 meV). For the purposes of the study, we considered a 7 Mbit 40 nm SRAM array with a layout cell area of 0.374 μm^2). We obtained an experimental thermal neutron-induced SER of 4 FIT/Mbit for the SRAM, with 75% of SBU, 17% of MCU with a multiplicity of 2 and 8% of events with multiplicities ranging from 3 to 5. All these MCU events correspond to physical adjacent bit cells in the memory plan. For comparison, results obtained with TIARA-G4 give a SER equal to 4.5 FIT/Mbit with 83% of SBU, 14% of MCU with a multiplicity of 2 and 4% of events with multiplicities ranging from 3 to 5.

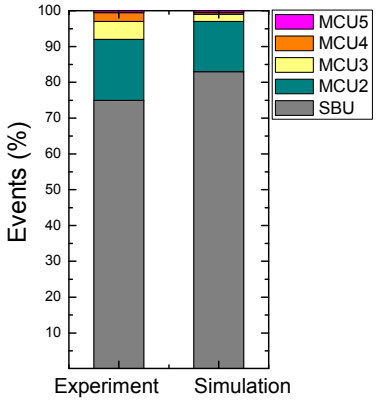

Figure 12. Event multiplicity distributions obtained for the 40 nm SRAM subjected to thermal neutrons and deduced from both experiment and numerical simulation, respectively conducted at LLB facility and obtained with the new release of the TIARA/Geant4 code.

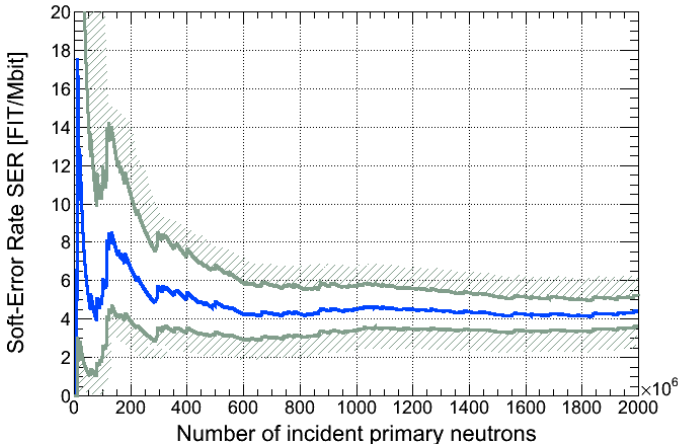

Figure 13. Convergence of the soft-error rate as a function of the number of incident primary neutrons obtained from TIARA-G4 simulation. The upper and lower limits of the SER confidence interval for 90% based on the χ^2 distribution are also plotted.

Figure 13 illustrates the convergence of the soft-error rate during the TIARA-G4 simulation as a function of the number of incident primary neutrons. The code asymptotically converges towards a unique SER value, demonstrating the invariance of the extracted SER when the statistics become satisfactory, typically above 1.5×10^9 primary neutrons in this case.

Finally, Figure 14 shows a synthesis of both experimental and simulation results obtained for the soft-error rate (expressed in bit flips) of the 40 nm single-port SRAM. “Simul. Part #1”, “Simul. Part #2” and “Simul. Part #3” correspond respectively to the SER extracted from

TIARA-G4 simulations considering the parts labeled #1, #2 and #3 of the reference atmospheric spectrum (Figure 1) as the primary sources of particles. Note that the contributions of parts #1 and #2 of the neutron spectrum in the SRAM SER are very small with respect to the high energy part #3 and only represent 3% of the total SER value. "Simul. 1+2+3" is equal to the sum of these three SER simulated values and corresponds to the SER estimation for the full atmospheric spectrum, estimated around 500 FIT/MBit. The "Exp. real-time ASTEP" value (682 FIT/Mbit) corresponds to the neutron-SER extracted from a real-time experiment (conducted on the ASTEP platform at the altitude of 2252m, see www.astep.eu) and corrected from the contribution of internal chip radioactivity (alpha-particle emission). The comparison of these results evidences a ~30% discrepancy between simulation and experimental results. Such an underestimation of the total SER by simulation in such ultra-scaled technology can be easily explained by the fact that the bipolar amplification mechanism has not been yet included in the SRAM electrical response module of the simulation code. In the next validation example (see subsection 5.2) considering a less integrated technology (65 nm), the impact of bipolar amplification will be significantly reduced and its impact on SER value quasi negligible.

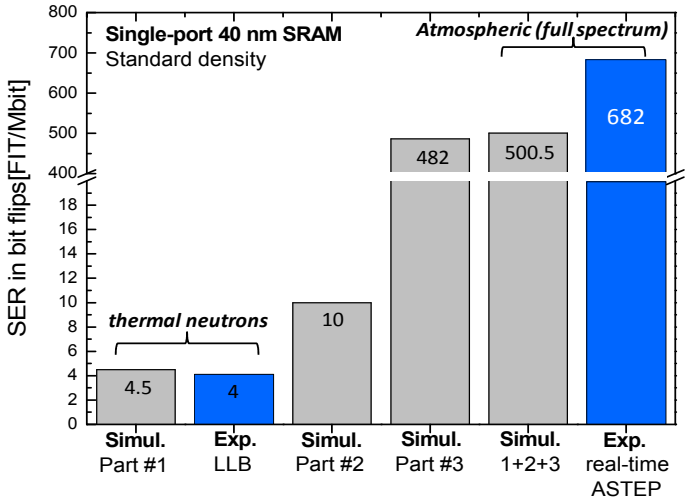

Figure 14. Synthesis of both experimental and simulation results obtained for the soft-error rate (expressed in bit flips) of the 40 nm single-port SRAM subjected to atmospheric neutrons.

5.2. SER estimation of a 65 nm SRAM under high energy atmospheric neutrons

In this second example, we simulated the complete 65 nm SRAM architecture previously defined in Figure 5. The objective was to compare neutron-induced SER results obtained by TIARA-G4 with simulation data previously obtained from the initial code TIARA [26,30] (see the introduction of section 4). Another objective was to perform simulation with and without taking into account the complete BEOL stack in order to evidence the impact of this BEOL on the neutron SER.

Figure 15 shows the comparison of the neutron-induced SER computed with the different versions of TIARA for a 20×20 65 nm SRAM array. The atmospheric neutron source considered for these simulations corresponds to the Part #3 of the reference neutron spectrum of Figure 1 (high energy neutrons below 1 MeV). Very close values are obtained with TIARA and TIARA-G4 without taking into account the complete BEOL structure (a single SiO_2 layer is used as a simplified BEOL stack in this case): respectively 266 and 251 FIT/MBit, evidencing the equivalence of the two approaches in terms of global SER values. For memory, the initial version of TIARA computes neutron-silicon interactions from pre-calculated databases using Geant4 while TIARA-G4 is a full Geant4 application. Taking into account the complete BEOL structure (defined in Figure 5) in the new code TIARA-G4 results in a significant increase of the SER (337 FIT/Mbit). This +30% variation of the SER can be attributed to additional secondary particles produced by the interactions of incoming neutrons with the different BEOL materials (mainly SiO_2, Cu and Al), these secondary particles being able to deposit electrical charges in the active silicon regions.

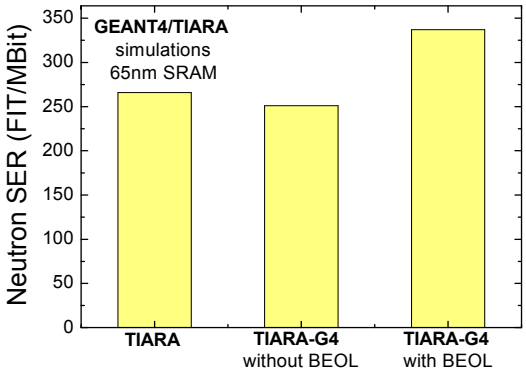

Figure 15. Comparison of simulation results obtained with the initial (TIARA) and new (TIARA-G4) versions of the code for the evaluation of the neutron-induced SER in the 65 nm SRAM architecture. Data are also plotted for TIARA-G4 with and without taking into account the real BEOL structure.

A more detailed analysis, reported in Figure 16, evidences slight differences in the distributions of the events as a function of the event size or event multiplicity (which corresponds to the number of simultaneous cell flips induced by a single primary particle interaction with the circuit). TIARA-G4 is found to generate more single bit upsets and, inversely, less multiple cell upsets than the initial TIARA code. The presence of the complete BEOL structure above silicon is also found to induce more single bit upsets and high multiplicity events than the simplified BEOL structure. This can be attributed to the production of new nuclei and recoil nuclei up to the atomic number Z = 74 corresponding to the tungsten, precisely present in the BEOL at the level of the plugs for the interconnection of drains with the first metal layer. The detailed analysis of this new produced nuclei shows that the majority of those inducing an upset are the result of neutron-cupper interactions in the first metal layers close to the active silicon.

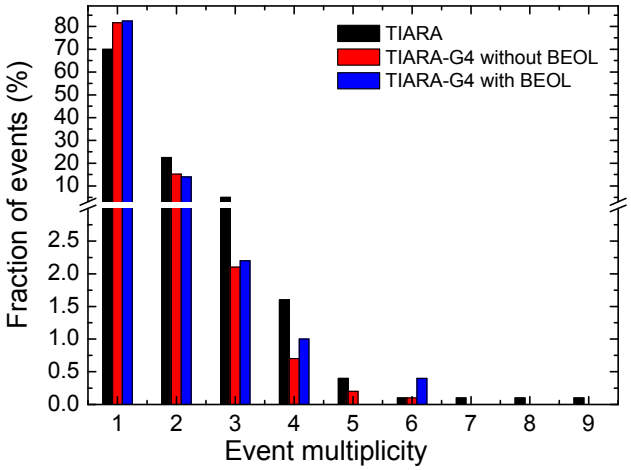

Figure 16. Event multiplicity distributions obtained with the initial (TIARA) and new (TIARA-G4) versions of the code for the evaluation of the neutron-induced SER in the 65 nm SRAM architecture. Data are also plotted for TIARA-G4 with and without taking into account the real BEOL structure.

5.3. Effects of low-energy muons on a 65 nm SRAM circuit

This last example concerns a preliminary study of the effects of low-energy muons on SRAM memories. As already introduced in subsection 2.1, atmospheric muons represent an important part of the natural radiation environment at ground level [1,20]. The muon is an elementary particle similar to the electron, with a unitary negative electric charge and a mass about 200 times the mass of an electron. The muon, denoted by μ^- and also called "negative muon", has a corresponding antiparticle of opposite charge and equal mass: the antimuon, often called "positive muon" (μ^+). Because they are charged, both negative and positive muons can loss their kinetic energy by ionization process when they travel through matter. But this interaction with matter is tenuous and muons can travel large distances in matter, thus deeply penetrating into material circuits.

Another particularity of muons is that they are unstable particles with a mean lifetime of 2.2 μs. They spontaneously decay into three particles:

$$\mu^- \rightarrow e^- + \overline{\upsilon}_e + \upsilon_\mu \qquad \mu^+ \rightarrow e^+ + \upsilon_e + \overline{\upsilon}_\mu . \tag{7}$$

Finally, when negative muons (and only negative muons) stop in silicon, about 35% decay following the previous reaction scheme and the remaining 65% are captured. If an intermediate state is assumed, the capture reaction can be written as:

$$\mu^- + Si^{28} \rightarrow Al^{28} + \nu + 100.5\ MeV \tag{8}$$

The excited ^{28}Al nucleus can decay from the following modes, thus producing secondary heavy nuclei that can deposit important charge in silicon:

$$\begin{aligned} Al^{28} &\rightarrow Al^{27} + n\,(12.4\ MeV) \\ &\rightarrow Al^{27} + n\,(14.2\ MeV) \\ &\rightarrow Na^{24} + \alpha\,(15.5\ MeV) \\ &\rightarrow Mg^{26} + d\,(18.4\ MeV) \end{aligned} \tag{9}$$

In contrast to the first version of TIARA, TIARA-G4 is now capable of simulating the impact of muons on SRAM circuits. For this first study, we considered low energy (< 1 MeV) negative and positive muons susceptible to directly deposit charge by ionization or to be captured (negative muons) after they stop in silicon. The Geant4 general particle source was then used to generate mono-energetic muons incident on the well-known 65 nm SRAM architecture (with complete BEOL) previously defined in Figure 5. Figure 17 illustrates different possible scenarios of negative and positive muon interactions with the structure. Figure 17(a) shows a negative muon decay in the top layers of the BEOL structure, this cannot lead to an upset since the muon disintegrates in light particles not able to deposit any significant charge in silicon. Figure 17(b) shows a similar event but occurring in the silicon substrate. In this case, the incoming positive muon traverses the complete BEOL structure and, statistically, can cross a sensitive drain. If the charge deposited in the impacted drain is higher than the critical charge for this transistor type and for this technology, the corresponding memory cell is upset. Figures 17 (c) and (d) show two negative muon capture events occurring in the BEOL and in silicon, respectively. These events produce large secondary particle showers, containing one or more charged particles susceptible to reach the active silicon region and to induce an upset or even a multiple cell upset. Of course, the probability to induce an upset is maximum when the muon capture-induce shower is produced in the immediate vicinity of the sensitive drain layer, as illustrated in Figure 17(d). This case corresponds to a reduced energy interval for the incoming muons in so far as the penetration depth of the muons in the structure and then the capture location primarily depends on the muon kinetic energy.

In order to illustrate this effect, we plotted in Figure 18 the distribution inside the SRAM structure of the vertex positions related to the negative muon capture reactions for three different values of the incident muon kinetic energy: 0.1, 0.3 MeV and 0.5 MeV. We clearly evidence in this figure such a dependency of the capture position (depth) with the muon kinetic energy. As a result, the soft error rate induced by negative muon irradiation presents a maximum when precisely muon captures occurs at the depth of the layer containing sensitive drains. This behavior is illustrated in Figure 19 which also plot the percentage of cell upsets induced by muon capture reactions or directly by muon impacts on sensitive drain (i.e. direct charge deposition in drain volumes). When increasing the kinetic energy of primary particles, the fraction of upsets induced by muon capture rapidly decrease as soon captures occur deeper in silicon, below the active layer. In this case, upsets become mainly induced by direct charge deposition from incident muons.

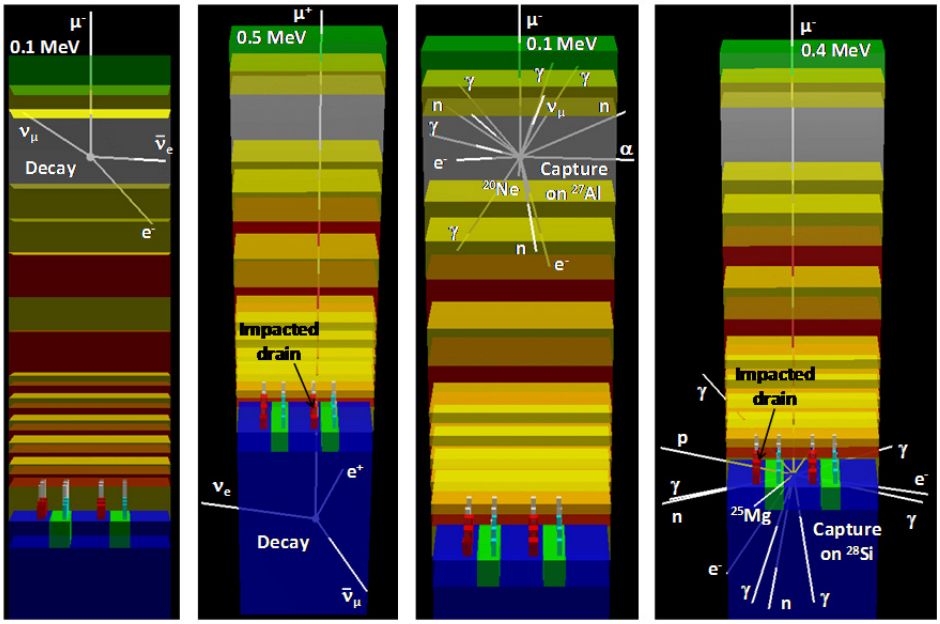

Figure 17. TIARA-G4 screenshots under ROOT of four events illustrating the interactions of low energy negative and positive muons with the complete 65 nm SRAM structure. From left to right: μ- decay in the BEOL (Al layer), μ+ upsetting a drain by direct charge deposition though the structure followed by the muon decay in the substrate, μ- capture on an aluminum atom in the BEOL, μ- capture on a silicon atom in the active circuit region (Pwell) leading to a drain upset via a direct impact by a secondary particle (proton in this case).

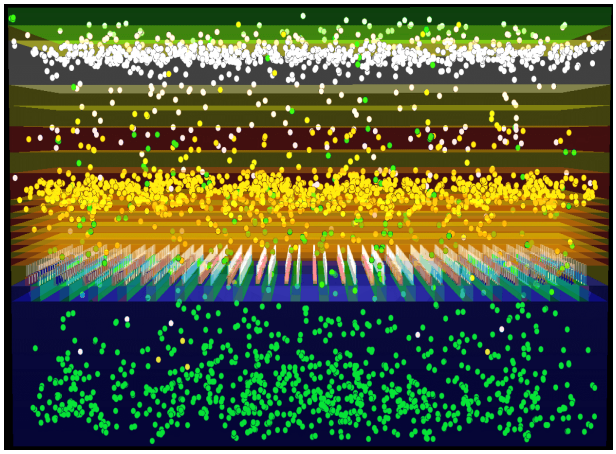

Figure 18. 3D distribution inside the SRAM circuit of the vertex positions related to the negative muon capture reactions for three different values of the incident muon kinetic energy: 0.1 MeV (white dots), 0.3 MeV (yellow dots) and 0.5 MeV (green dots).

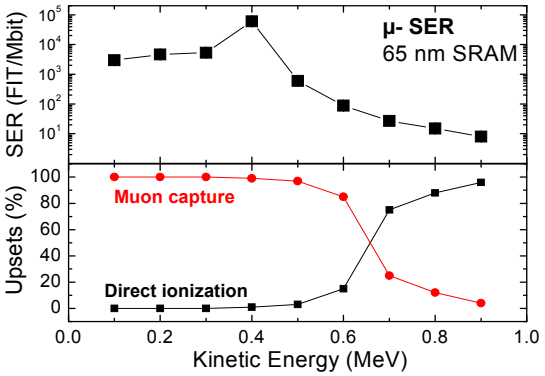

Figure 19. Estimated negative muon-induced soft error rate versus muon kinetic energy for the 65 nm SRAM. The percentage of cell upsets induced by the secondary particles produced by muon capture reactions or directly by muon impacts on sensitive drain (i.e. direct charge deposition in drain volumes) are also plotted.

6. Conclusion

In conclusion, we described in this chapter a new simulation platform, named TIARA-G4, we have developed these last years for the numerical evaluation of the sensitivity of advanced semiconductor memories (static RAMs) subjected to natural radiation at ground level. Based on the Geant4 toolkit, the application is sufficiently general and modular to simulate a user-defined circuit architecture subjected to the external irradiation by heavy-ions, neutrons, protons, muons or directly by alpha-particles generated inside the circuit materials. After defining the natural radiation environment at ground level and the different types of radiation constraints, we presented in details the different modules of our code, including the methods and approximations adopted to model the circuit architecture, to generate particles mimicking a given radiation environment and to model the circuit/cell electrical response. Finally, we illustrated the capabilities of our code to estimate the soft-error rate in deca-nanometer SRAM circuits subjected to atmospheric thermal and high energy neutrons and to mono-energetic positive and negative muons, investigating and illustrating for the first time, some unconventional physical effects, such as the ^{10}B thermal neutron capture at the level of the Pmos drains or the negative muon capture and its consequences on the SER in the SRAM circuit structure. TIARA-G4 should be used in the future to more deeply investigate the radiation response of ultimate MOS circuits and alternate nanoelectronic devices in the natural (terrestrial) environment.

Author details

Jean-Luc Autran, Sergey Semikh , Daniela Munteanu and Sébastien Serre
Aix-Marseille University & CNRS, Marseille, France

Gilles Gasiot and Philippe Roche
STMicroelectronics, Crolles, France

7. References

[1] J.F. Ziegler, H. Puchner, SER – History, Trends and Challenges, Cypress Semiconductor, 2004. See also references therein.

[2] M. Nicolaidis (Editor), Soft Errors in Modern Electronic Systems, Springer (2010).

[3] J.L. Leray, "Effects of atmospheric neutrons on devices, at sea level and in avionics embedded systems", Microelectronics Reliability, Volume 47, Issues 9-11, pp. 1827-1835, 2007.

[4] S. Mitra, P. Sanda, and N. Seifert, "Soft Errors: Technology Trends, System Effects and Protection Techniques," IEEE VLSI Test Symposium, 2008.

[5] R.C. Baumann, "Radiation-Induced Soft Errors in Advanced Semiconductor Technologies", IEEE Transactions on Device and Material Reliability, Vol. 5, pp. 305-316 (2005).

[6] R. D. Schrimpf, D. M. Fleetwood (Editors), Radiation Effects And Soft Errors In Integrated Circuits And Electronic Devices, World Scientific Publishing (2004).

[7] E. Normand, "Single Event Upset at Ground Level", IEEE Trans. Nucl. Sci., Volume NS-43, N°6, pp. 2742-2750, 1996. See also references therein.

[8] D.F. Heidel, P.W. Marshall, K.A. LaBel, J.R. Schwank, K.P. Rodbell, M.C. Hakey, M.D. Berg, P.E. Dodd, M.R. Friendlich, A.D. Phan, C.M. Seidleck, M.R. Shaneyfelt, M.A. Xapsos, "Low Energy Proton Single-Event-Upset Test Results on 65 nm SOI SRAM", IEEE Trans. Nucl. Sci., vol 55, Issue 6, pp. 3394-3400, 2008.

[9] E. H. Cannon, M. Cabanas-Holmen, J. Wert, T. Amort, R. Brees, J. Koehn, B. Meaker, and E. Normand, "Heavy Ion, High-Energy, and Low-Energy Proton SEE Sensitivity of 90-nm RHBD SRAMs", IEEE Trans. Nucl. Sci., vol 56, Issue 7, pp. 3493-3499, 2010.

[10] J. F. Dicello, C. W. McCabe, J. D. Doss, and M. Paciotti, "The relative efficiency of soft-error induction in 4K static RAMs by muons and pions", IEEE Trans. Nucl. Sci., vol 30, Issue 6, pp. 4613-4616, 1983.

[11] C. J. Gelderloos1i, R. J. Peterson, M. E. Nelson, and J. F. Ziegler, "Pion-Induced Soft Upsets in 16 Mbit DRAM Chips", IEEE Trans. Nucl. Sci., vol 44, Issue 6, pp. 2237-2242, 1997.

[12] S. Duzellier, D. Falguère, M. Tverskoy, E. Ivanov, R. Dufayel, and M.C. Calvet, "SEU Induced by Pions in Memories From Different Generations", IEEE Trans. Nucl. Sci., vol 48, Issue 6, p. 1960-1965, 2001.

[13] Brian D. Sierawski, Marcus H. Mendenhall, Robert A. Reed, Michael A. Clemens, Robert A. Weller, Ronald D. Schrimpf, Ewart W. Blackmore, Michael Trinczek, Bassam Hitti, Jonathan A. Pellish, Robert C. Baumann, Shi-Jie Wen, Rick Wong, and Nelson Tam, "Muon-Induced Single Event Upsets in Deep-Submicron Technology", IEEE Trans. Nucl. Sci., vol. 57, issue 6, pp. 3273-3278, 2011.

[14] Sierawski, B.D.; Reed, R.A.; Mendenhall, M.H.; Weller, R.A.; Schrimpf, R.D.; Wen, S.; Wong, R.; Tam, N.; Baumann, R.C, "Effects of scaling on muon-induced soft errors", International Reliability Physics Symposium (IRPS 2011), pp. 3C3.1-6.

[15] J.L. Autran, D. Munteanu, P. Roche, G. Gasiot, S. Martinie, S. Uznanski, S. Sauze, S. Semikh, E. Yakushev, S. Rozov, P. Loaiza, G. Warot, M. Zampaolo, "Soft-errors induced

by terrestrial neutrons and natural alpha-particle emitters in advanced memory circuits at ground level", Microelectronics Reliability, Vol. 50, pp. 1822-1831 (2010).
[16] P. E. Dodd, "Device Simulation of Charge Collection and Single-Event Upset", IEEE Trans. Nucl. Sci., vol. 43, no. 2, pp. 561-575, April 1996.
[17] P.E. Dodd and L.W. Massengill, "Basic mechanisms and modeling of single-event upset in digital microelectronics", IEEE Trans. Nucl. Sci., vol. 50, no. 3, pp. 583–602, Jun. 2003.
[18] P. E. Dodd, "Physics-Based Simulation of Single-Event Effects", IEEE Trans. Device Mater. Reliab., vol. 5, no. 3, pp. 343-357, Sept. 2005.
[19] D. Munteanu, J.L. Autran, "Modeling of digital devices and ICs submitted to transient irradiations", IEEE Trans. Nucl. Sci., 2008, Vol. 55, no. 4, pp. 1854-1878.
[20] L.I. Dorman, Cosmic Rays in the Earth's Atmosphere and Underground, Kluwer Academic Publishers, 2004.
[21] M.S. Gordon, P. Goldhagen, K.P. Rodbell, T.H. Zabel, H.H.K. Tang, J.M. Clem, P. Bailey, " Measurement of the Flux and Energy Spectrum of Cosmic-Ray Induced Neutrons on the Ground", IEEE Trans. Nucl. Sci., Vol. 1, 2004, pp. 3427-3434.
[22]] F. Lei, S. Clucas, C. Dyer, P. Truscott, "An atmospheric radiation model based on response matrices generated by detailed Monte Carlo Simulations of cosmic ray interactions", IEEE Trans. Nucl. Sci., 2004, Vol. 51, pp. 3442-3451.
[23] F. Lei, A. Hands, S. Clucas, C. Dyer, P. Truscott, "Improvement to and Validations of the QinetiQ Atmospheric Radiation Model (QARM)", IEEE Trans. Nucl. Sci., 2006, Vol. 53, pp. 1851-1858. See also http://qarm.space.qinetiq.com/
[24] F. Wrobel, J. Gasiot, F. Saigné, A. D. Touboul, "Effects of atmospheric neutrons and natural contamination on advanced microelectronic memories", Appl. Phys. Lett., Vol. 93, 064105, 2008.
[25] G. Adamiec and M. Aitken, "Dose-rate conversion factors: update", Ancient TL, Vol. 16, N°2, pp. 37-50, 1998.
[26] S. Uznanski, G. Gasiot, P. Roche, C. Tavernier, J-L. Autran, "Single Event Upset and Multiple Cell Upset Modeling in Commercial Bulk 65 nm CMOS SRAMs and Flip-Flops," IEEE Trans. Nucl. Sci., vol. 57, issue 4, pp. 1876-1883, Aug 2010.
[27] S. Uznanski, G. Gasiot, P. Roche, J. L. Autran, "Combining GEANT4 and TIARA for Neutron Soft Error Rate Prediction of 65 nm Flip-Flops," IEEE Trans. Nucl. Sci., vol. 58, issue 6, pp. 2599-2606, Dec 2011.
[28] S. Agostinelli et al., "Geant4—a simulation toolkit", Nuclear Instruments and Methods in Physics Research Section A: Accelerators, Spectrometers, Detectors and Associated Equipment, Vol. 506, pp.250-303, 2003.
[29] SRIM software, available online: http://www.srim.org/
[30] S. Uznanski, "Monte-Carlo simulation and contribution to understanding of Single Event Upset (SEU) mechanisms in CMOS technologies downto 20nm technological node.", Ph.D. Thesis, Aix-Marseille University, Sept. 2011.
[31] Geant4 General Particle Source, http://reat.space.qinetiq.com/gps/
[32] JEDEC Standard Measurement and Reporting of Alpha Particles and Terrestrial Cosmic Ray-Induced Soft Errors in Semiconductor Devices, JESD89 Arlington, VA: JEDEC Solid State Technology Association.

[33] T. Sato, H. Yasuda, K. Niita, A. Endo and L. Sihver "Development of PARMA: PHITS-based Analytical Radiation Model in the Atmosphere", Radiation Research, 2008, Vol. 170, pp. 244-259.

[34] EXcel-based Program for calculating Atmospheric Cosmic-ray Spectrum, available online at http://phits.jaea.go.jp/expacs/index.html

[35] U. Bravar, E.O. Flückiger, K. Godin, Z.C. Hansen, J.R. Macri, M.L. McConnell, R.S. Miller, M. R. Moser, J.M. Ryan, "Atmospheric Neutron Measurements with the SONTRAC Science Model", IEEE Nuclear Science Symposium Conference Record, 2005, N14-126.

[36] J. Kempa and I.M. Brancus, "Zenith angle distributions of cosmic ray muons", Nuclear Physics B - Proceedings Supplements, 2003, Vol. 122, pp. 279-281.

[37] http://Geant4.web.cern.ch/Geant4/support/proc_mod_catalog/physics_lists/referencePL.shtml

[38] ROOT, an object oriented framework for large scale data analysis, available online: http://root.cern.ch

[39] J.M. Palau, G. Hubert, K. Coulie, B. Sagnes, M.C. Calvet, S. Fourtine, "Device Simulation Study of the SEU Sensitivity of SRAMs to Internal Ion Tracks Generated by Nuclear Reactions", IEEE Trans. Nucl. Sci., Vol. 48, N°2, pp. 225-231, 2001.

[40] G. Hubert, A. Bougerol, F. Miller, N. Buard, L. Anghel, T. Carriere, F. Wrobel, R. Gaillard, "Prediction of Transient induced by Neutron/Proton in CMOS combinational Logic Cells", Proceedings of the 12th IEEE International On-Line Testing Symposium (IOLTS'06).

[41] R. Baumann, T. Hossain, S. Murata, H. Kitagawa, "Boron Compounds as a Dominant Source of Alpha Particles in Semiconductor Devices," IEEE International Reliability Physics Physics Symposium, 1995, pp. 297-302.

[42] R. Baumann and E. Smith, "Neutron-Induced 10B Fission as a Major Source of Soft Errors in High Density SRAMs", Microelectronics Reliability, Vol. 41, 2001, pp. 211-218.

[43] M. Olmos, R. Gaillard, A. Van Overberghe, J. Beaucour, S.Wen, S. Chung, "Investigation of thermal neutron induced soft error rates in commercial SRAMs with 0.35 μm to 80 nm technologies", IEEE International Reliability Physics Physics Symposium, 2006, pp. 212-216.

[44] S. Wen, R. Wong, M. Romain, N. Tam, "Thermal neutron soft error rate for SRAM in the 90-45 nm technology range", IEEE International Reliability Physics Physics Symposium, 2010, pp. 1036-1039.

[45] Laboratoire CEA-CNRS Léon Brillouin (LLB), http://www-llb.cea.fr/